Shear and normal load perturbations on a two-dimensional continuous fault: 1. Static triggering

H. Perfettini
Laboratoire de Géophysique Interne et Tectonophysique, Grenoble, France

J. Schmittbuhl
Laboratoire de Géologie, École Normale Supérieure, Paris, France

A. Cochard
Laboratoire de Détection et de Géophysique, Commissariat ál'Energie Atomique, Bruyères-le-Châtel, France
Laboratoire de Géologie, École Normale Supérieure, Paris, France

Received 31 January 2002; revised 28 August 2002; accepted 2 April 2003; published 3 September 2003.

[1] The influence of normal and shear stress static perturbations on a strike-slip fault is addressed on the basis of a two-dimensional continuous and quasi-dynamic model. Friction along the fault plane is described using a rate-and-state friction law with depth variable properties. Normal and shear stress perturbations result in similar effects in terms of earthquake triggering if $\Delta\tau - \mu_*\Delta\sigma$ is constant, $\Delta\tau$ and $\Delta\sigma$ being the amplitude of the shear and normal stress fluctuations, respectively, and μ_* being a constant which can be interpreted as the static friction coefficient on the fault in a Coulomb failure model. Therefore the Coulomb stress change $\Delta CFF = \Delta\tau - \mu_*\Delta\sigma$ is a useful tool to account simultaneously for normal and shear stress variations in our model. We also show that when estimating the clock advance or clock delay of an earthquake, the simple Coulomb failure model is at first order in good agreement with our results during the first 90% of the earthquake cycle. However, it differs significantly during the last 10% due to the sharp velocity increase predicted by the rate-and-state friction law before rupture. This suggests that as long as static variations of stress are concerned, realistic fault models using rich, laboratory-based, friction laws like rate-and-state friction laws may lead to predictions fairly close to the ones made using one of the simplest failure model, i.e., the Coulomb failure model. This may explain why Coulomb stress change computations, although often based on drastic approximations, have been able in many occasions to explain earthquake triggering sequences. *INDEX TERMS:* 7209 Seismology: Earthquake dynamics and mechanics; 7215 Seismology: Earthquake parameters; 7260 Seismology: Theory and modeling; *KEYWORDS:* earthquake triggering, static triggering, Coulomb stress change, rate and state friction laws, clock advance/delay

Citation: Perfettini, H., J. Schmittbuhl, and A. Cochard, Shear and normal load perturbations on a two-dimensional continuous fault: 1. Static triggering, *J. Geophys. Res.*, *108*(B9), 2408, doi:10.1029/2002JB001804, 2003.

1. Introduction

[2] Knowing the timing of an earthquake with accuracy represents one of the most fundamental goals of earthquake physics but seems for the moment like an impossible task. However, a major advance would be to predict the locations and timing of the aftershocks of a given main shock. For this reason, earthquake triggering has been a widely studied phenomenon in the last decade.

[3] Computation of the static Coulomb stress change [see *King et al.*, 1994] after a major earthquake appears as a useful tool since it seems that an important percentage of the aftershocks lies in areas where the Coulomb stress has increased while seismicity seems to be reduced in the stress shadows [*Harris and Simpson*, 1998] where Coulomb stress decreases. Even though this static tool has been successful in modeling the earthquake sequence of Landers [*King et al.*, 1994] and on the North Anatolian fault [*Stein et al.*, 1997], it fails to explain the existence of triggered seismicity at large distances from the Landers epicenter [e.g., *Gomberg et al.*, 2001], where the static stress changes are negligible. The physical mechanism that seems responsible for such a remote triggering is the passage of seismic waves [see, e.g., *Gomberg and Bodin*, 1994; *Gomberg and Davis*, 1996; *Gomberg et al.*, 2000b], which induces significant but transient stress perturbations at large distance from the main shock.

[4] In order to understand the triggering processes, we propose to study the effect of permanent (static stress field) as well as transient (dynamic stress field) variations of both

0148-0227/03/2002JB001804$09.00

shear and/or normal stresses on the triggering of earthquakes and link them to Coulomb stress changes. Static triggering is studied in the present paper. Transient variations are addressed in the companion paper by *Perfettini et al.* [2003]. *Dieterich* [1994] and *Gomberg et al.* [1998] have considered permanent as well as transient perturbations of the shear stress using the simple spring slider fault model in absence of inertial effect. A similar study has been carried on by *Roy and Marone* [1996] considering inertia by giving a mass to the slider. We extend here these previous studies to both shear and normal stress perturbations, and propose to use a more realistic fault description that takes into account long range elastic interactions. For this purpose, we use a two-dimensional (2-D) continuous model of a strike-slip fault with depth variable frictional properties (see Figure 1a), analogous to the model of *Rice* [1993]. The model is quasi-dynamic in the sense of *Rice* [1993] (stress changes due to slip are static and propagate instantaneously; an instantaneous radiation damping term is included, in order to prevent infinite velocities during instabilities). Instead of assigning a mass to the fault as in the work of *Roy and Marone* [1996] in order to prevent instability, we use the physically based radiation damping term that has two advantages: (1) it damps the slip instability and (2) its existence is derived from the laws of elastodynamics. Note that in a spring slider model, the inertial term is proportional to the time derivative of the velocity of the slider (term in $m\dot{V}(t)$, where $V(t)$ is the sliding velocity) while the radiation term is proportional to the fault velocity (term in $GV(t)/2\beta$, where G is the shear modulus and β is the shear wave velocity). This model has been compared to a full dynamic model by *Lapusta et al.* [2000] and *Lapusta and Rice* [2003] showing that both models are in good agreement. The quasi-dynamic simulation preserves the main features of the dynamic simulation. However, our goal is not to study in detail earthquake rupture but rather to look at the onset of instability where most, if not all, dynamic effects may be neglected. In contrast with previous studies, the model rigorously accounts for the simultaneous temporal variations of the shear and normal stresses. Accordingly, the total Coulomb stress change can be computed. Sensitivity to normal stresses fluctuations has also been included in the friction law along the fault. We use a laboratory-based, rate-and-state friction law with a state variable that depends on the normal stress fluctuations [*Linker and Dieterich*, 1992].

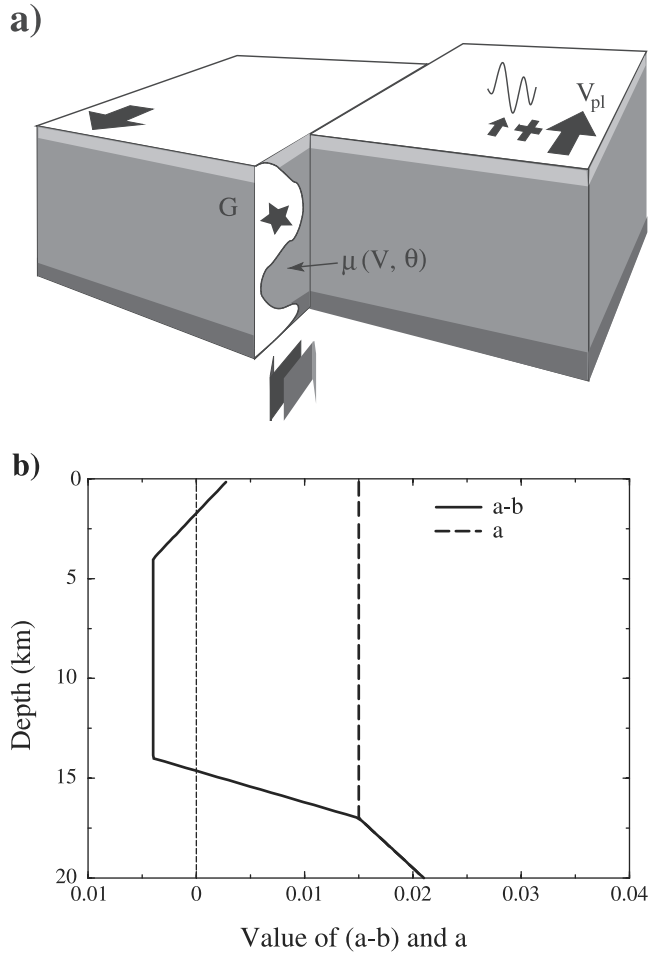

Figure 1. (a) Sketch of the fault geometry used in this model. The fault of friction coefficient μ and rigidity G is invariant along strike (2-D fault model) but has depth-dependent frictional properties. Stress perturbations are added to the loading due to the motion of the plates at velocity V_{pl}. (b) Frictional parameters a (dashed line) and $a - b$ (solid line) as a function of depth. The shallow (-2 km $< z < 0$) as well as the deepest part ($z > -14.7$ km) of the fault show velocity strengthening ($a > b$) while at intermediate depths (-14.7 km $< z < -2$ km), the fault has a velocity weakening behavior.

2. Rate-and-State Friction Laws

[5] Rate-and-state friction laws [*Dieterich*, 1979; *Ruina*, 1983] have been successfully used to model a wide range of phenomena from rock friction experiment laboratory measurements [*Dieterich*, 1979, 1981], to the entire earthquake cycle including earthquake afterslip [*Tse and Rice*, 1986; *Marone et al.*, 1991; *Lapusta and Rice*, 2003].

[6] Under this formalism, the coefficient of friction $\mu = \tau/\sigma$, where τ and σ are the shear and normal stress, respectively on the fault, may be expressed as

$$\mu(V,\theta) = \mu_* + a\ln\left(\frac{V(t)}{V_*}\right) + b\ln\left(\frac{\theta(t)}{\theta_*}\right), \qquad (1)$$

where $V(t)$ is the sliding velocity, $\theta(t)$ is a state variable which may be physically interpreted as the average age of the population of contacts between the two bare surfaces [*Dieterich*, 1981; *Persson*, 1998], and a and b are some empirical constants, while V_*, θ_*, and μ_* are reference values such as $\mu(V_*, \theta_*) = \mu_*$. The logarithmic terms in equation (1) may be justified by a thermally activated process [e.g., *Baumberger et al.*, 1999].

[7] The evolution of the state variable with time is given by the Dieterich evolution or "ageing" law

$$\dot{\theta} = 1 - \frac{V(t)\theta(t)}{D_c}\ , \qquad (2)$$

where D_c, a characteristic length, may be understood as the average length for the renewal of the population of contacts, i.e., the average size of such a contact.

[8] When the sliding velocity reaches zero, the evolution law (2) shows, assuming a proper regularization of

equation (1), that $\dot{\theta} = 1$ and θ may be interpreted as the time of contact. Other experimentally based evolution laws exist such as the Ruina or "slip" law:

$$\dot{\theta} = -\frac{V(t)\theta(t)}{D_c}\ln\frac{V(t)\theta(t)}{D_c}, \tag{3}$$

but we will not consider them since they lack a physical interpretation and are more difficult to deal with analytically.

[9] A steady state exists that is reached when $\dot{\theta} = 0$, i.e., $\theta = \theta_{ss} = D_c/V$, where the subscript *ss* refers to steady state. In this case, the coefficient of friction becomes

$$\mu_{ss} = \mu_* + (a-b)\ln\left(\frac{V(t)}{V_*}\right). \tag{4}$$

Examination of equation (4) shows that the coefficient of friction at steady state is decreasing with increasing sliding velocity when $b > a$ while the opposite happens when $a > b$. Therefore velocity weakening ($b > a$) surfaces are potentially unstable and able to generate stick-slip instabilities or earthquakes while velocity strengthening surfaces ($a > b$) promote stable sliding or creep. The word potentially is introduced since the fault surface is surrounded by an elastic medium which may, in the velocity weakening case, stabilize slip if stiff enough (see section 4).

[10] *Linker and Dieterich* [1992] and later *Richardson and Marone* [1999] showed that the rate-and-state formalism still holds in the case of variable normal stress, the equation of the state variable evolution being changed to

$$\dot{\theta} = 1 - \frac{V\theta}{D_c} - \alpha\frac{\theta\dot{\sigma}}{b\sigma}, \tag{5}$$

where a new parameter α is introduced.

[11] The value of the frictional parameters a, b, μ_*, D_c and α can be obtained from laboratory friction experiments. However, it is not clear whether such values are relevant at the fault scale. We now briefly discuss this issue.

[12] 1. The confinement of seismicity at intermediate depths is consistent with the temperature dependence of the quantity $a - b$ as inferred from laboratory experiments [*Blanpied et al.*, 1991]. Therefore we believe that laboratory estimates of a and b can be extrapolated at the fault scale without any changes.

[13] 2. If rate-and-state effects were to be ignored ($a = b = 0$), then μ_* would represent the constant coefficient of friction of the fault in a simple Coulomb failure model. Such a quantity is not well known at the fault scale. However, its estimate by the mean of, say, Coulomb stress computations (see the review of *Harris* [1998]) as well as deep well in situ measurements [e.g., *Brudy et al.*, 1997] are comparable with values inferred from laboratory experiments.

[14] 3. Using a simple friction model based on the Bowden-Tabor theory of friction (i.e., all the contacts between the two surfaces are independent and identical, and have reached the yield plastic stress) [*Bowden and Tabor*, 1950, 1964], *Perfettini* [2000] found that $\alpha \simeq \mu_*/3$. *Linker and Dieterich* [1992] and *Richardson and Marone* [1999] have measured the α parameter on granite surfaces with gouge. They both found $\alpha \simeq 0.2$ and μ_* 0.6, which is in agreement with the estimate $\alpha \simeq \mu_*/3$.

[15] 4. The most delicate point concerns the parameter D_c. When measured on bare rock surfaces in the laboratory, D_c varies in the range 1–10 μm which is consistent with the average size of the contacts as measured by *Dieterich and Kilgore* [1994] by imaging surface contacts. When a gouge zone is introduced, the value of D_c increases, and on the basis of their laboratory measurements, *Marone and Kilgore* [1993] propose that $D_c = 1$ mm for the San Andreas fault. A recent experiment by *Chambon et al.* [2002] conducted in a shear rotary apparatus with a wide gouge zone (of the order of 0.1 m), even suggests that D_c could be of the order of several decimeters, which is of the order of the estimate obtained by inversion of teleseismic daa [*Ide and Takeo*, 1997; *Bouchon et al.*, 1998]. The actual value of D_c for faults is still the focus of many discussions and cannot yet be accurately estimated (see *Uenishi and Rice* [2002, section 5.2] for a discussion). Because of numerical constraints, we will choose D_c values of the order of a centimeter, as discussed in section 4.

3. Model

[16] We consider a strike-slip fault invariant along strike (see Figure 1a). Therefore we deal with a 2-D antiplane fault with variable properties with depth. For the sake of simplicity a quasi-dynamic approximation is used, i.e., dynamic effects are only considered through the presence of a radiation damping term (see below) that prevents infinite velocities during instability. The existence of the free surface is taken into account using a mirror image of the fault. The model is therefore similar to the one described by *Rice* [1993]. The numerical domain of width $2L$ (the factor of 2 being due to the use of the mirror image) is divided into n cells of length $\Delta x = 2L/n$ for which slip, slip velocity and stress are computed at the center of each cell. Under the rate-and-state formalism, the frictional stress at point i depends on the slip velocity $V_i(t)$, the state variable $\theta_i(t)$, but also on the normal stress $\sigma_i(t)$:

$$\tau_i[V_i(t),\theta_i(t),\sigma_i(t)] = \sigma_i(t)\,\mu_i[V_i(t),\theta_i(t)], \tag{6}$$

where the coefficient of friction at point i can be expressed as

$$\mu_i[V_i(t),\theta_i(t)] = \mu_i^* + a_i\ln\left(V_i(t)/V_*\right) + b_i\ln\left(\theta_i(t)/\theta_*\right). \tag{7}$$

The state evolution of the ith cell is described by

$$\dot{\theta}_i(t) = \psi_i[V_i(t),\theta_i(t),\sigma_i(t),\dot{\sigma}_i(t)], \tag{8}$$

where the functional $\psi_i[V_i(t), \theta_i(t), \sigma_i(t)]$ reads

$$\psi_i[V_i(t),\theta_i(t),\sigma_i(t),\dot{\sigma}_i(t)] = 1 - \frac{V_i(t),\theta_i(t)}{D_{c_i}} - \frac{\alpha_i\,\theta_i(t)}{b_i}\frac{\dot{\sigma}(t)}{\sigma(t)}, \tag{9}$$

following *Linker and Dieterich* [1992].

[17] Considering the well-known relation between a slip distribution $\delta(x)$ over an antiplane fault and its associated quasi-static shear stress variation $-(G/(2\pi))\int_0^L(\partial\delta(\xi)/\partial\xi)/(x-\xi)\,d\xi$ [e.g., *Bilby and Eshelby* 1968], where G is the shear modulus, ξ an integration variable which covers the

whole fault length L, i.e., $0 < \xi < L$. In our particular model the absolute shear stress on the fault can be written as

$$\tau(x,t) = \tau^0(x,t) - \frac{G}{2\beta}\left(V(x,t) - V_{pl}\right) - \frac{G}{2\pi}\int_0^L \frac{1}{x-\xi} \cdot \frac{\partial[\delta(\xi,t) - V_0 t]}{\partial\xi} d\xi + \Delta\tau(x,t)\ , \quad (10)$$

where β is the shear wave speed and V_{pl} is the plate velocity.

[18] The first term on the right-hand side represents the initial stress on the fault $\tau^0(x)$, the second one is the radiation damping term, and the third term represents the above mentioned elastic interactions. Temporal variations of the shear stress are taken into account through the $\Delta\tau(x, t)$ term. Now, assuming that all fields are constant over each grid cell of length Δx, which amounts to writing $\delta(\xi, t) = \Sigma_j \delta_j(t)\{H[\xi - (j - 1/2)\Delta x] - H[\xi - (j + 1/2)\Delta x]\}$, where H is the Heaviside function, the discretized version (10) reads

$$\tau_i[V_i(t), \theta_i(t), \sigma_i(t)] = \tau_i^0 - \frac{G}{2\beta}\left[V_i(t) - V_{pl}\right] + \Sigma_{j=1}^n K_{ij}\left[\delta_j(t) - V_{pl}\, t\right] + \Delta\tau_i(t), \quad (11)$$

where the spatial x dependence is replaced by the discrete i dependence and the static kernel K_{ij} is given by

$$K_{ij} = \frac{G}{2\pi\Delta x}\left[\frac{1}{(i-j)^2 - 1/4}\right]. \quad (12)$$

[19] Describing the evolution of the system requires to solve a system of n equations (one for each point of the fault) such as equation (11). This may be done using an implicit scheme [e.g., *Dieterich*, 1992; *Rice*, 1993]. Like *Stuart and Tullis* [1995], we prefer to rearrange the set of equations in order to use an explicit scheme. Deriving equation (11) at cell i with respect to time reads

$$(\partial\tau_i/\partial V_i)\,\dot{V}_i + (\partial\tau_i/\partial\theta_i)\,\dot{\theta}_i + (\partial\tau_i/\partial\sigma_i)\,\dot{\sigma}_i = -\frac{G}{2\beta}\,\dot{V}_i + \Sigma_{j=1}^n K_{ij}\left(V_j - V_{pl}\right) + \Delta\dot{\tau}_i(t). \quad (13)$$

Since $\dot{\theta}_i = \psi_i$ and $\partial\tau_i/\partial\sigma_i = \mu_i$, the system of 2 n first order differential equations to be solved is

$$\begin{cases} \dot{V}_i(t) = \left[\Sigma_{j=1}^n K_{ij}\left(V_j - V_{pl}\right) - (\partial\tau_i/\partial\theta_i)\,\psi_i - \mu_i\dot{\sigma}_i + \Delta\dot{\tau}_i(t)\right] \Big/ \left[\partial\tau_i/\partial V_i + \frac{G}{2\beta}\right] \\ \dot{\theta}_i(t) = \psi_i[V_i(t), \theta_i(t), \sigma_i(t), \dot{\sigma}_i(t)], \end{cases} \quad (14)$$

where i runs from 1 to n. This set of equations is integrated using a Runge-Kutta algorithm [*Press et al.*, 1992] with a fifth-order adaptive step-size control. Such an explicit procedure is much faster (and easier to implement) than an implicit one. Also note that, due to the translational invariance of the kernel K (i.e., the value of K_{ij} only depends on $i - j$), the summation in equation (14) reduces to a convolution which can be computed using fast Fourier transform methods.

[20] As mentioned above, fault properties are only depth-dependent. The fault of length L = 20 km is loaded at constant velocity V_{pl} = 35 mm/yr. The shear wave velocity is β = 3 km/s and the shear modulus is G = 30 GPa. For the sake of simplicity, normal stress is held constant to σ_0 = 50 MPa throughout the depth. Such a case corresponds to high fluid overpressurization at depth, as discussed by *Rice* [1992]. The model includes a free surface boundary at z = 0 km.

[21] The frictional parameters a and b are allowed to vary with depth in agreement with *Blanpied et al.* [1991]. This variation is mainly caused by the dependence on temperature (and so on depth) of the laboratory-inferred a and b parameters at large depths, while it is likely to be due to a transition from consolidated ($z < -2$ km) to unconsolidated ($z > -2$ km) gouge at shallow depths [e.g., *Marone*, 1998]. The values of the a and $a - b$ parameters versus depth shown in Figure 1b were taken from *Lapusta and Rice* [2003, and references therein]. Both the shallow and the deep part of the fault show velocity strengthening ($a > b$), while at intermediate depths, the fault has velocity weakening properties ($b > a$). This intermediate part is the seismogenic zone of our model.

[22] The α parameter of *Linker and Dieterich* [1992] is set to α = 0.2 except when b = 0 ($z < -$ 17km). Since the derivative of θ with respect to time given in equation (5) has no meaning when b reaches 0, we set α = 0 when b = 0, in order to eliminate this pathological case. The constant term $\mu_*(z)$ in the coefficient of friction was held constant at $\mu_*(z) = \mu_* = 0.6$ as well as the constant reference velocity V_* which was set to $V_* = 1$ μm/s.

4. Stability and Nucleation Size

[23] Some of the features of the 2-D model can be captured using a simplified 1-D model often referred to as the spring block model. In this model, the elasticity of the medium is reduced to a spring of stiffness k. The equations of motion of the 1-D fault are (here the block is assumed massless)

$$\begin{cases} \dot{V} = \left[k\left(V_{pl} - V\right) - (\partial\tau/\partial\theta)\psi - \mu\,\dot{\sigma} + \dot{\Delta\tau}(t)\right] \Big/ [\partial\tau/\partial V] \\ \dot{\theta} = \psi[V(t), \theta(t), \sigma(t)]. \end{cases} \quad (15)$$

A comparison between the 1-D and 2-D model is given by H. Perfettini et al. (manuscript in preparation, 2002). The equivalent stiffness of the fault k per unit area, is defined in our model by

$$k = \Gamma G/L, \quad (16)$$

where L is the length of the fault. Equation (16) is a general property of elastic systems (e.g., *Dieterich* [1992] or *Rice* [1993]). The constant Γ is of the order of unity (we choose $\Gamma = 2/\pi$ as discussed by H. Perfettini et al. (manuscript in preparation, 2002). [2002]) and depends on the geometry of the fault and on the deformation mode. This scaling of the fault stiffness has some fundamental consequences, as will be discussed below.

[24] Stability analysis performed by *Rice and Ruina* [1983] using the spring block model shows that for a velocity weakening friction ($b > a$), the slider exhibits stable slip for $k > k_c$ and unstable slip for $k < k_c$, the critical stiffness being given by $k_c = \sigma_0(b - a)/D_c$, with σ_0 the normal load. Recalling the scaling $k = \Gamma\ G/L$ where L is the length of the fault, this implies that a fault of size $L < L_c$ shows stable slip while a fault of length $L > L_c$ undergoes unstable slip, i.e., stick-slip motion. The critical length L_c, often called the nucleation length, is given by $L_c = \Gamma\ G/k_c = \Gamma\ GD_c/[\sigma_0(b - a)]$.

[25] According to this concept of nucleation size, the minimum size of an earthquake is L_c since no instability can occur for faults smaller than L_c. To study the effect of temporal perturbations of the loading stress, two type of faults have to be considered.

[26] The first type consists of faults smaller than the nucleation size L_c. These faults do not produce earthquakes since they slip in a stable way. The question to ask is: Are perturbations of the loading stress able to destabilize these faults? This point has been extensively discussed by *Perfettini et al.* [2001] considering a spring slider model and is extended to a 2-D continuous fault model by H. Perfettini et al. (manuscript in preparation, 2002).

[27] The second type consists of faults bigger than the nucleation size L_c. These faults are unstable and therefore seismically active. The question to ask is: Will the perturbations of the loading stress hasten or delay the occurrence of the earthquake? This point will be discussed in section 6 and is the aim of this work.

[28] The characteristic length D_c of the friction law is set in our model to $D_c = 2$ cm at all depths. The choice of this value is mainly dictated by numerical reasons. As first pointed out by *Rice* [1993], a proper discretization of a continuous fault involves a grid spacing Δx much smaller than the nucleation size in order to properly account for the nucleation process. Since we have $L_c = (2/\pi)[GD_c/\sigma_0(b - a)]$ in our model, we find, taking $b - a = 0.004$ as in the seismogenic zone, that $D_c = 2$ cm implies $L_c \simeq 2$ km. Taking $L_c \gtrsim 10\Delta x$ for a proper discretization, this calls for about 100 elements to discretize the fault, hence about $n \sim 200$ elements to discretize the whole numerical domain of length $2L$. In most of our numerical runs, we choose $n = 256$ grid points, thus insuring a correct resolution of the continuum at minimum time consumption, allowing us to widely explore the parameter space of our model.

5. Numerical Procedure

[29] We start all our numerical simulations with a fault at the steady state, i.e., $V_i = V_{pl}$, $\sigma_i = \sigma_0$, and $\theta_i = D_c/V_{pl}$ for all points of the fault. At time $t = 0$, an earthquake is artificially nucleated, the sliding velocity being suddenly increased by a factor of 10 in the region $[z_0 - L_c/2; z_0 + L_c/2]$ with $z_0 = -10$ km. We then let the fault evolve with time. The maximum sliding velocity $V_{\max}$ over the whole fault is shown as a function of time in Figure 2 for $n = 256$ grid points. The fault rapidly enters a stationary regime where earthquakes occur periodically. This regime appears to be independent of the particular choice of the artificial nucleation procedure. With our choice of parameters, the interseismic time is of the order of $T_{\text{inter}} \simeq 96.2$ years. The slip distribution for two events is shown in Figure 3 which further emphasizes the similarity between events. The events nucleate at 5 km, propagate, and finally rupture the fault between the surface and about 16 km depth.

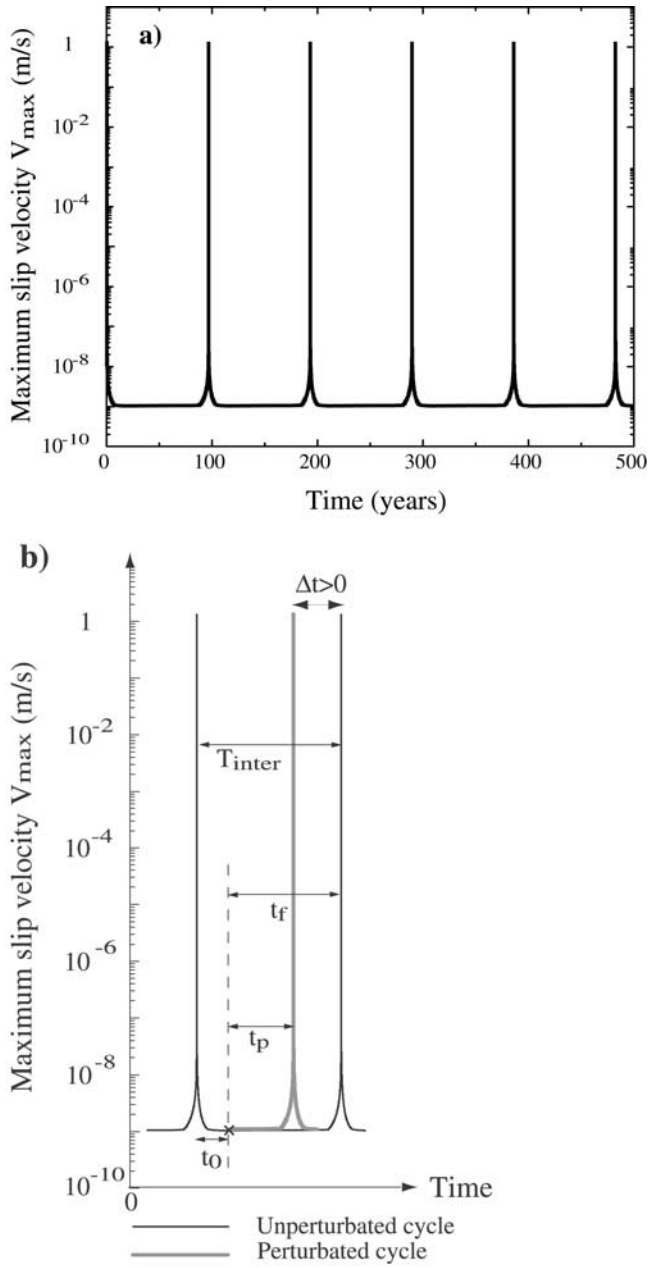

Figure 2. (a) Maximum sliding velocity on the fault as a function of time. (b) Sketch defining the times used in this study. T_{inter} is total duration of the earthquake cycle, t_f is unperturbated time to failure, t_p is time to failure when stress perturbations are considered, t_0 is time of application of the perturbation, and $\Delta t = t_f - t_p$ is the clock change.

[30] Once the fault has reached a stationary regime, we save the value of the velocity V_i and state variable θ_i at given times of the earthquake cycle for all points of the fault. These values are then used as initial conditions for runs that include perturbations.

[31] Perturbations may change the duration of the rest of the cycle, t_p, which is denoted t_f in the absence of perturba-

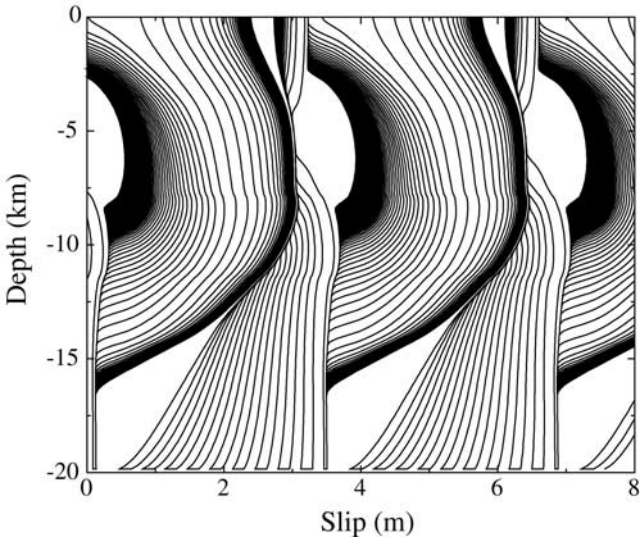

Figure 3. Slip as a function of depth. Each line represents the slip distribution at a given time and corresponds to a velocity change of 10%.

tions and is considered as a reference ($T_{\mathbf{inter}} = t_0 + t_f$, see Figure 2b). Clock advance or clock delay Δt are estimates of the difference between the duration after perturbation, t_p, and the reference duration t_f : $\Delta t = t_f - t_p$. A clock advance corresponds to a positive Δt and a clock delay to a negative Δt. The initiation time t_0 is measured from the onset of the cycle and the durations t_f or t_p are times to instability from t_0. Instability is declared when the maximum slip velocity on the fault surpasses a prescribed threshold of 10^{-2} m/s. This value is in agreement with the order of magnitude of the velocity V_{in} at the transition from quasi-static to dynamic slip inferred by *Roy and Marone* [1996] considering a spring slider model and accounting for inertial effects. Indeed, they found that $10^{-3} < V_{in} < 10^{-1}$ m/s, a value that brackets our slip velocity threshold 10^{-2} m/s. Note, that due to the abrupt increase of the sliding velocity at the end of the earthquake cycle, the choice of this velocity threshold has almost no effect in terms of predicted clock change.

6. Static Triggering (ST)

[32] When the transient change of the loading stress due to the passage of the seismic wave has ceased, a static stress perturbation is left on the fault. The object of this paper is the effect of such a permanent change in the loading stress. As in the work by *Gomberg et al.* [1998], we model these variations as stress steps. A stress step is defined by its amplitude and its time of application t_0. We first consider the effect of loading steps, that is, steps that promote failure.

[33] The model allows the use of shear and normal stress perturbations. In order to describe perturbations with a single parameter, we introduce the Coulomb failure function:

$$\mathrm{CFF}(\tau, \sigma) = \tau - \mu_\star \sigma, \tag{17}$$

where $\mu_\star$ is the reference friction coefficient introduced in equation (1). We used $\mu_* = 0.6$. Time derivability of the stress step is obtained using a sine evolution over a time interval of 10 s. Discussion of the friction coefficient choice is included in section 7.

[34] Accordingly, stress perturbations are described as $\Delta\mathrm{CFF}(\Delta\tau, \Delta\sigma) = \Delta\tau - \mu_\star\Delta\sigma$. We first consider only normal stress perturbations: $\Delta\mathrm{CFF}(0, \Delta\sigma)$. Complete perturbations of $\Delta\mathrm{CFF}(\Delta\tau, \Delta\sigma)$ of both shear and normal stress are addressed in section 6.3.

6.1. Loading Steps (ΔCFF > 0)

6.1.1. Influence of Triggering Time t_0

[35] We first consider the influence of the time t_0 at which the loading step is applied. Figure 4 shows the clock advance due to normal loading steps applied at various times t_0 for two step magnitudes ΔCFF. The amplitude of the normal stress steps are $\Delta\sigma = -0.005$ and -0.5 MPa (10^{-4}% and 10^{-2}%, respectively, of the total normal load σ_0). We see that the clock advance is roughly constant when $t_0 \lesssim 90$ years. Small magnitude fluctuations of broad wavelength ($\sim$20 years) are superimposed and their existence is discussed in Appendix A. The later the triggering time t_0, the larger the departure from a constant approximation. For very late perturbation triggering ($t_0 \gtrsim 90$ years), the clock advance falls down and reaches the instantaneous triggering curve for which $\Delta t = t_f$.

[36] The straight lines in Figure 4 represent the prediction of the Coulomb failure model which predicts a clock advance of

$$\Delta t_{\mathrm{CFF}} = \Delta\mathrm{CFF}/\dot{\tau}, \tag{18}$$

where $\dot{\tau}$ is the loading stress rate. However, the clock advance in our work is obtained using the formula $\Delta t = \min(\Delta t_{\mathrm{CFF}}, T_{\mathbf{inter}} - t_0)$ where $T_{\mathbf{inter}}$ is the duration of the earthquake cycle and t_0 the time at which the static load is applied. Indeed, the clock advance can not exceed the time left until the next event $t_f = T_{\mathbf{inter}} - t_0$ when no perturbations are considered. We see in Figure 4 that the limit $\Delta t = T_{\mathbf{inter}} - t_0$ is strictly followed only for large stress fluctuations ($\Delta\sigma = -0.5$ MPa). For smaller magnitude of the stress perturbation ($\Delta\sigma = -0.005$ MPa), there is a departure from the Coulomb failure approximation but also from the instantaneous triggering curve $\Delta t = T_{\mathbf{inter}} - t_0 = t_f$.

[37] The loading stress rate $\dot{\tau}$ is equal in the spring slider model to $\dot{\tau} = kV_{pl}$, where k is the equivalent stiffness of the fault defined in equation (16). We see that during most of the cycle, the prediction of the simple Coulomb failure model is in good agreement with our results derived using a rate-and-state friction law. However, the Coulomb failure model is unable to explain the small oscillation of the clock advance observed in Figure 4, which are discussed in Appendix A.

6.1.2. Influence of the Step Amplitude ΔCFF

[38] We now study the influence of the amplitude ΔCFF of the loading stress steps for normal stress steps $\Delta\sigma < 0$. Figure 5 presents the clock advance as a function of the amplitude of the steps ΔCFF applied at three different times $t_0 = 14$, 54 and 94 years. The most important observation of Figure 5 is that the clock advance is proportional to the amplitude of the steps. The Coulomb failure model leads to the clock advance Δt_{CFF} and this prediction (straight line in Figure 5) is in good agreement with the 2-D continuous fault model.

[39] The predictions of the Coulomb failure model differ significantly from the numerical calculations when the steps

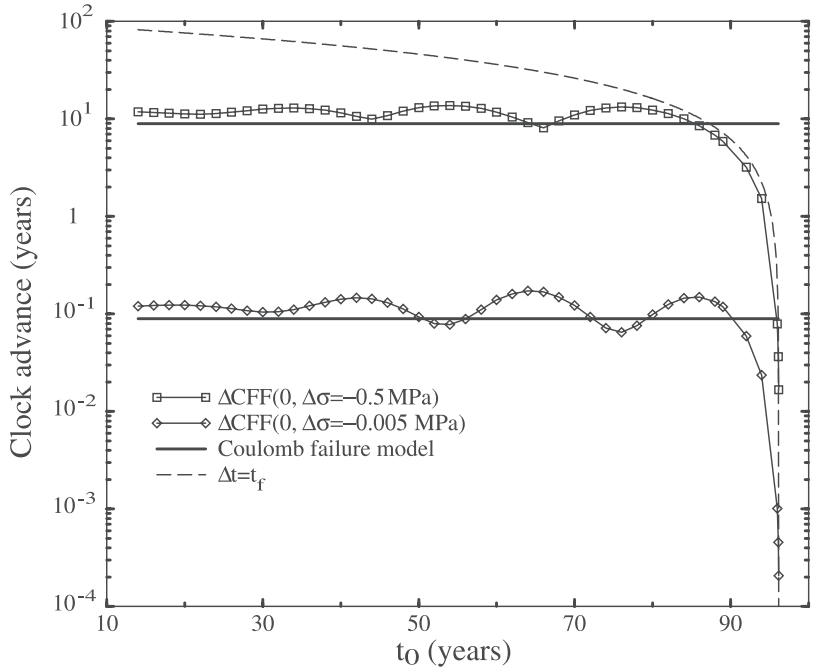

Figure 4. Clock advance due to loading steps in normal stress as a function of perturbation triggering time t_0. Estimates of the clock advance for two magnitudes of the normal stress perturbation: ΔCFF (0, Δσ = 0.5 MPa) and ΔCFF(0, Δσ = 0.005 MPa) are plotted. The Coulomb failure model (straight lines) appears as a good first order approximation of the continuous 2-D fault model. The dashed line corresponds to the maximum possible clock advance $\Delta t = t_f$ or instantaneous triggering. The earthquake normally occurs at time t = 96.2 years in the absence of perturbations.

are applied late in the cycle (t_0 = 94 years) as may be seen in Figure 5. At those times, the non linearities of the friction law become important due to the rapid increase of the sliding velocity. This effect is lacking in a Coulomb failure model where the fault is always at rest (V = 0) during the interseismic period. It explains the large discrepancy (in terms of predicted clock change) between the prediction of the Coulomb failure criterion and our results. The cutoff because of the maximum clock advance also introduces a significant departure from the Coulomb failure criterion. Subsequently, the clock advance due to a step applied very late in the cycle might be smaller by several orders of magnitude than the clock advance due a step applied early in the cycle. Unlike transients variations of stress [see *Perfettini et al.*, 2003], static variations of stress have a higher triggering potential when applied early in the cycle. As previously noted by *Gomberg et al.* [1998], this is due to the fact that the earlier the permanent perturbation is applied, the bigger its effect. However, we emphasize that during most of the cycle (i.e., before the late departure from the Coulomb failure criterion, that is, $t_0 \lesssim 90$ years), the clock advance is weakly sensitive to the triggering time t_0 since it shows a plateau with small amplitude fluctuations (see Figure 4).

6.2. Unloading Steps (Δcff < 0)

6.2.1. Influence of Triggering Time t_0

[40] Unloading steps (ΔCFF(Δτ, Δσ) < 0) may delay the occurrence of rupture. Figure 6 represents the clock delay $-\Delta t$ due to normal stress steps of amplitude Δσ = 0.5 MPa and Δσ = 0.005 MPa applied at various times t_0. It is crucial to note that unlike clock advance, clock delay is unbounded. There is no cutoff at late triggering time t_0 since the clock delay is not related to the duration t_f. As for the loading steps (see Figure 5), the clock delay is roughly constant as long as $t_0 < 90$ years. Small magnitude oscillations also exist with an increasing magnitude with triggering time t_0. Their origin is discussed in Appendix A. The Coulomb failure model (straight line in Figure 5) predicts a clock delay equal to

$$\Delta t_{\mathrm{CFF}} = -\Delta \mathrm{CFF}/\dot{\tau}, \tag{19}$$

which is independent of the triggering time t_0. It is again in good agreement with the numerical results for steps applied early in the cycle ($t_0 \lesssim 90$ years) but differs for steps applied late in the cycle ($t_0 \gtrsim 90$ years).

[41] The sensitivity of the clock advance and clock delay to the triggering time t_0 may also be understood from the following equation (20) obtained from Appendix D2. It gives an expression of the clock change due to a stress step of small amplitude, i.e., $\Delta\tau \ll a\sigma_0$ applied at time t_0:

$$\Delta t = \Delta t_{\mathrm{CFF}}\left[1 - \frac{\exp(\gamma t_0)}{1 + \frac{\gamma a}{\dot{\delta}_0 H}}\right], \tag{20}$$

with $\gamma = \dot{\tau}_0/(a\sigma_0)$, $H = b/D_c - k/\sigma_0$ (k is the equivalent stiffness of the fault), and $\dot{\delta}_0$ is the initial sliding velocity. This expression was obtained using the spring slider model. Looking at equation (20), we see that the clock advance differs from the Coulomb prediction (see equation (19)) by a factor $\Delta t/\Delta t_{\mathrm{CFF}} = 1 - \{\exp(\gamma t_0)/[1 + (\gamma\, a\dot{\delta}_0 H)]\}$. The bigger t_0, the larger the discrepancy between the Coulomb

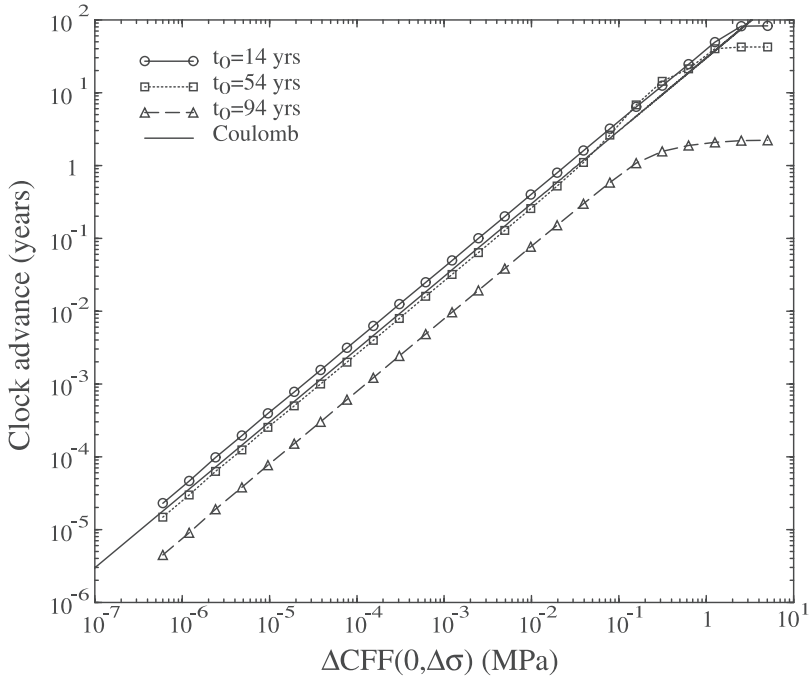

Figure 5. Clock advance as a function of the amplitude of a loading step $\Delta CFF(0, \Delta\sigma < 0)$ applied at three triggering times t_0 = 14, t_0 = 54, and t_0 = 94 years. Prediction from the Coulomb failure model (straight line) is in good agreement with our results for early triggering time t_0. For late triggering (t_0 = 94 years), the cutoff because of the maximum clock advance ($\Delta_t \leq t_f$) becomes dominant.

failure model and the prediction of a 1-D model that obeys rate-and-state friction.

6.2.2. Influence of the Step Amplitude

[42] Figure 7 presents the clock delay due to normal stress steps of various amplitudes, all of them being applied either at time t_0 = 14 (early), or t_0 = 54 (middle), or t_0 = 94 years (late in the cycle). We observe that the clock delay is proportional to the amplitude of the steps. The prediction of the Coulomb failure model (straight line) Δt_{CFF} (see equation (19)) is in very good agreement with numerical simulations. We note that the departure from the Coulomb failure model prediction increases for late triggering. This is consistent with

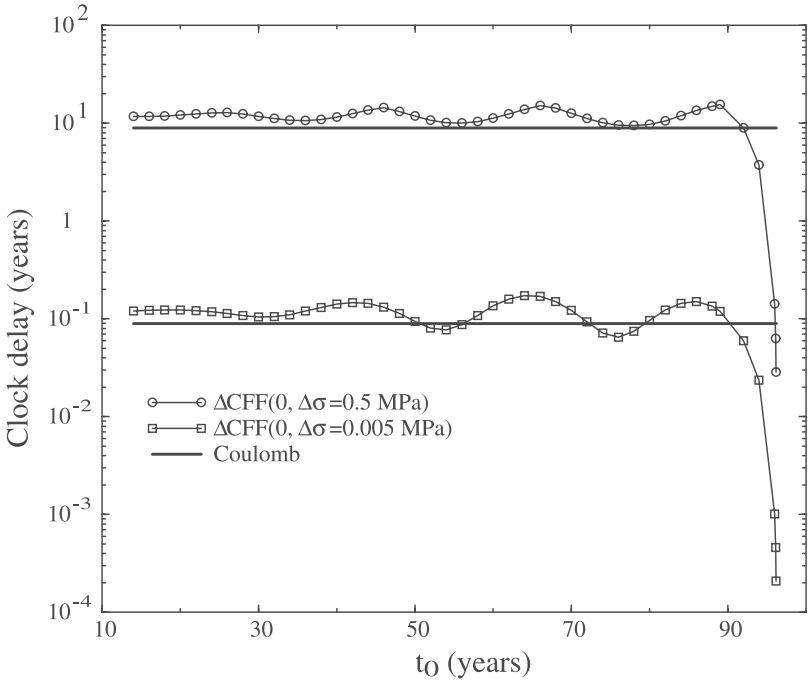

Figure 6. Same as Figure 4 for unloading steps.

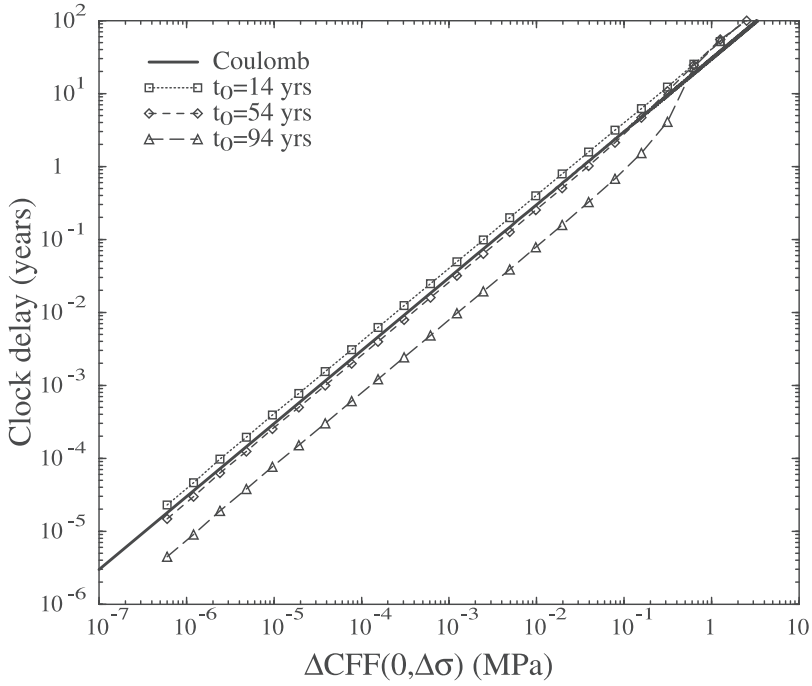

Figure 7. Clock delay as a function of the amplitude of an unloading step ($\Delta\sigma > 0$) applied at three different triggering times $t_0 = 14$, $t_0 = 54$, and $t_0 = 94$ years for various normal stress steps. The prediction of the Coulomb failure model Δt_{CFF} (straight line) is in agreement with the numerical calculations for not too late triggering time t_0.

equation (20) which shows that the above mentioned factor, i.e., $\Delta t/\Delta t_{CFF}$, decreases from one for late triggering.

[43] When stress steps are applied late in the cycle, the predictions of the Coulomb failure model differ significantly from numerical calculation results at low step amplitudes ($\Delta_{CFF} < 0.5$ MPa) but are in good agreement at higher amplitudes. This discrepancy may be understood in the following way. At low amplitudes, the spring block approximation leads to a clock delay of $-\Delta t$ where Δt is given in equation (20). Therefore the vertical downward shift in a log-log diagram (Figure 7), of the clock delay $-\Delta t$ with respect to the Coulomb failure prediction (see equation (19)) is $1 - \exp(\gamma\, t_0)/[1 + (\gamma\, a/\dot{\delta}_0 H)]$. However, for unloading steps of high amplitude, the clock delay can be obtained using equation (D8), leading to

$$-\Delta t = \Delta t_{CFF} + \frac{1}{\gamma}\log\left[1 - \frac{\exp(\gamma t_0)}{1 + \frac{\gamma a}{\dot{\delta}_0 H}}\right] . \qquad (21)$$

At first order, the first term of the right hand (Δt_{CFF}) is dominant. Accordingly, the ratio $\Delta t/\Delta t_{CFF}$ is close to one and the shift, in a log-log diagram, is in this case zero, the numerical results being in agreement with the Coulomb failure model. Therefore we explain both behaviors for low and high unloading amplitude steps and their different consistency with the prediction of the Coulomb failure model.

6.3. Normal and/or Shear Stress Perturbations ($\Delta\tau$ and/or $\Delta\sigma$)

[44] In the previous sections we considered permanent variations of the normal stress (loading or unloading step). In this section we extend our results to perturbations of the shear stress. We show that a large combination of stress perturbations are equivalent. They have to fulfill the following criterion:

$$\Delta\mathrm{CFF}(\Delta\tau, \Delta\sigma) = \mathrm{const} . \qquad (22)$$

[45] Figure 8 shows the clock advance Δt for four cases of stress perturbations at constant ΔCFF: only a shear stress perturbation (0.1 MPa, 0), only a normal stress perturbation ($0, -0.1/\mu_*$ MPa), and two mixed cases ($0.025, -0.075/\mu_*$) and ($0.075, -0.025/\mu_*$). The four numerical curves perfectly superimpose and show that the relevant description of static stress perturbations has to be done using the Coulomb stress perturbation ΔCFF. A similar conclusion can be drawn from the clock delay estimate. This result is extended for dynamic perturbations by *Perfettini et al.* [2003].

[46] A last result concerns the relationship between advance and delay when changing the sign of the Coulomb stress perturbation. At a given triggering time t_0, we computed the clock advance for a perturbation $\Delta\mathrm{CFF} = -0.5$ MPa and the clock delay for $\Delta\mathrm{CFF} = 0.5$ MPa. The ratio of the advance and the delay is plotted in Figure 9 with respect to the triggering time t_0. We see from Figure 9 that the triggering of a loading or unloading stress step at a given time t_0 does not lead to a "symmetric" situation. Delay and advance are not of the same magnitude. The later the triggering, the larger the difference between advance and delay might be. This result might have implications for inhibition or enhancement of stress Coulomb modeling. Indeed, a region with mixed conditions of Coulomb stress perturbations might see a strong enhancement of the clock

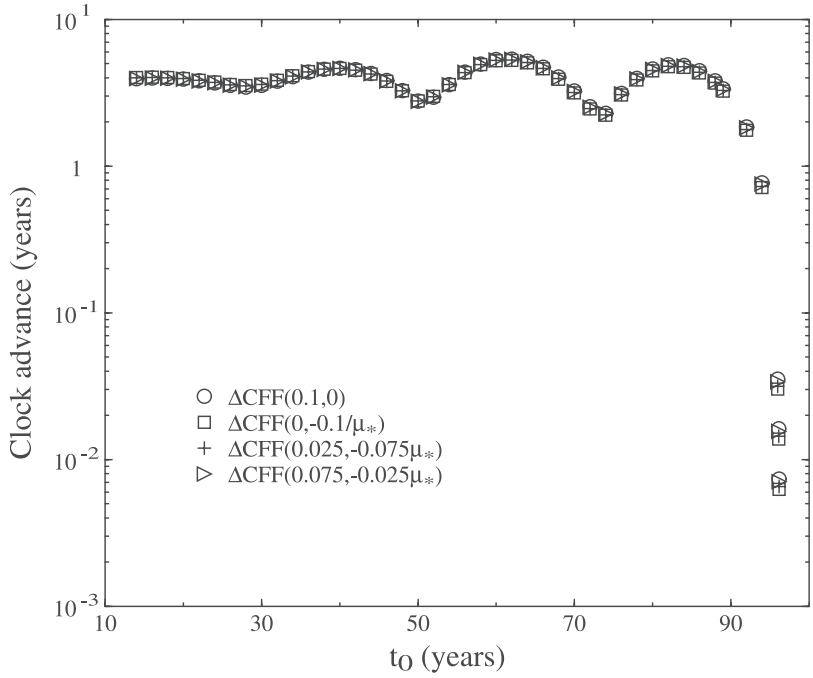

Figure 8. Clock advance as a function of the triggering time t_0 for different stress perturbations at constant ΔCFF = 0.1 MPa.

advance if other regions of clock delay are relatively inhibited, i.e., large ratio advance/delay.

7. Discussion

[47] As discussed in section 1, the computation of the static Coulomb stress changes has been successful in explaining a large number of earthquake sequences (see *Harris* [1998] for a review). We discuss this success in the view of our results.

[48] First, we showed that for most types of perturbations, normal and shear stress variations have the same effect in terms of clock advance if their amplitudes satisfy $\Delta\text{CFF} = \Delta\tau - \mu_*\Delta\sigma = \text{Const}$.

[49] This observation may be justified using equation (B7) which gives the relative change of velocity following steps in normal and shear stress. As long as the normal stress variations are small, i.e., $\Delta\sigma \ll \sigma_0$, the influence of $(\sigma_1/\sigma_0)^{\alpha/a}$ is negligible and the relative change of velocity is given by

$$\frac{\Delta V}{V_0} \simeq \exp\left[\Delta\text{CFF}^0/(a\sigma_1)\right] - 1, \qquad (23)$$

where $\Delta\text{CFF}^0 = \Delta\tau - \mu_0\Delta\sigma$ is the Coulomb stress calculated using the coefficient of friction $\mu(t_0) = \mu_0$ at the time t_0 at which the stress step is applied.

[50] We now discuss the difference between ΔCFF^0 computed using μ_0 (which evolves during the earthquake cycle) and ΔCFF used all along the manuscript, that refer to the constant value μ_*. The latter friction coefficient μ_* is the reference friction coefficient (see equation (1)). The coefficient of friction $\mu(V, \theta)$ is roughly constant during the earthquake cycle but varies near the end of the cycle where it drops to lower values. The mean value of the coefficient of friction varies from 0.56 during seismic rupture to a peak value of 0.6 at the onset of instability. Accordingly the assumption $\mu_0 \simeq \mu_*$ is acceptable. Therefore the introduction of the Coulomb failure function $\Delta\text{CFF} = \Delta\tau - \mu_*\Delta\sigma$ is a relevant approximation which is confirmed by our results.

[51] As shown in section 6.3, the clock advance is uniquely defined for a given value of ΔCFF, despite the combinations of shear and normal stresses considered. This means that the Coulomb failure function is an efficient tool to account for simultaneous static variations of the shear and

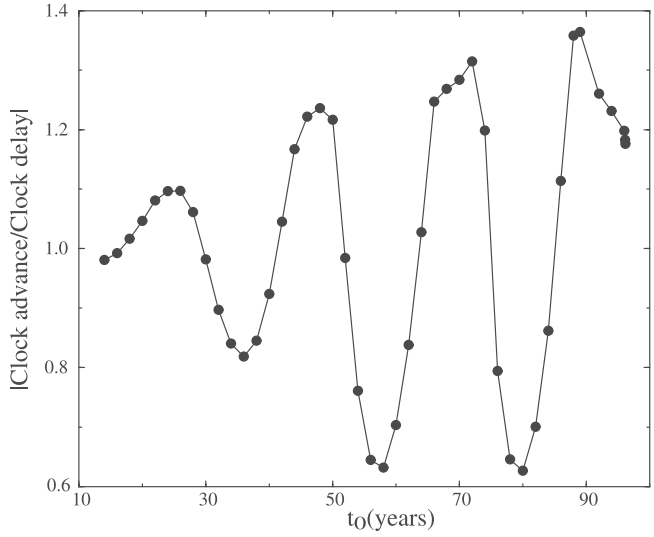

Figure 9. Ratio of the clock advance and clock delay as a function of the triggering time. Advance and delay are computed for the same magnitude of the stress perturbation $|\Delta\text{CFF}| = 0.5$ MPa but changing its sign.

normal load. The coefficient μ_* could be approximately considered as the constant coefficient of friction in a Coulomb failure model. We use the word "approximately" since μ_* depends on the sliding velocity for which it was measured, that is, V_*. Using $\mu'_* = \mu_* - a\log(V_*) - b\log(D_c/V_*)$ (with a and b being values representative of the seismogenic depths) might be more appropriate since it does not depend on the reference velocity V_*. However, since a and b are small compared to μ_*, the difference between μ'_* and μ_* is usually negligible ($\mu'_* \simeq 0.62$ instead of $\mu_* = 0.6$ in our work).

[52] In Appendix B we show that the Coulomb failure function can be extended to include the sensitivity to normal stress fluctuations of the state variable in the friction law. From equation (B14) and as previously proposed by *Dieterich* [1994], we define the Coulomb failure function as

$$\Delta CFF^{\alpha} = \Delta\tau - (\mu_0 - \alpha)\Delta\sigma, \tag{24}$$

where α is the normal stress sensitivity (see equation (5)).

[53] The second point is whether or not the Coulomb failure criterion is appropriate for earthquake mechanics. Of course, the answer is negative when one deals with transient stress perturbations or earthquake rupture. However, in section 6 we showed that except at the very end of the earthquake cycle (say the last 10% and for the case of unloading steps), the prediction of the Coulomb failure criterion in terms of clock advance or clock delay were in agreement to first order (i.e., neglecting the small oscillations) with our results when static variations of the loading stress were considered. The discrepancy between our results and the predictions of the Coulomb model at the end of the earthquake cycle comes from the fact that the coefficient of friction shows significant variations at the end of the cycle. We believe that the large period of agreement during the cycle may explain the success of the Coulomb failure criterion in modeling many earthquake sequences. In Appendix B we show that a fault governed by rate-and-state friction laws is Coulomb-like during the locked phase (i.e., when $V\theta/D_c \ll 1$). This phase lasts for most of the cycle [*Gomberg et al.*, 2000a]. Large positive ΔCFF reduces the duration of the locked phase and therefore, the departure from a Coulomb-like behavior occurs earlier in the cycle (see Figure 5). An opposite conclusion is reached when large negative steps in ΔCFF are considered. Indeed, large unloading steps increase the duration of the locked phase since the fault is slowed down. Therefore the departure from a Coulomb-like behavior occurs later in the cycle (see the $t_0 = 94$ year curve on Figure 7 at large amplitudes) in a phase called the self-accelerating phase [*Dieterich*, 1992]. The transition from the locked to the self-accelerating phase occurs when the state variable becomes greater than its steady state value, i.e., when $\theta > \theta_{ss} = D_c/V$. Using equation (1), this last inequality can be expressed as $\mu > \mu_{ss}$, where μ_{ss} is the coefficient of friction at steady state described in equation (4). Therefore the fault is in the locked phase as long as its coefficient of friction is lower than its steady state value, and evolves otherwise in the self-accelerating phase.

[54] However, one of the major differences between the predictions of the Coulomb failure model and our results is that at the end of the earthquake cycle, the clock delay due to unloading steps drops to zero. Such a feature has been previously noticed by *Harris and Simpson* [1998] considering the effect of the 1906 San Francisco earthquake on the seismicity of the bay area. In particular, the 1911 $M > 6.0$ earthquake near Morgan Hill occurred in a stress shadow of the 1906 event that is in an unloaded area (ΔCFF < 0). *Harris and Simpson* [1998] found that rate-and-state time-to-failure calculations are consistent with the occurrence of the 1911 earthquake if the Calaveras fault was already close to failure before the 1906 event. In other words and in agreement with our results, a fault at the end of the earthquake cycle seems to be only slightly sensitive to external stress perturbations, the nucleation process being underway.

[55] The last point we discuss is the possible existence of a threshold amplitude for static triggering. A lower bound for this threshold was found to be 0.01 MPa [*King et al.*, 1994; *Harris*, 1998] and corresponds to the onset of a positive correlation between the presence of aftershocks and an increase of the Coulomb stress (ΔCFF > 0). However, a recent study by *Ziv and Rubin* [2000], considering 63 $M \geq 4.5$ earthquakes in central California, did not exhibit a threshold in this region.

[56] The existence of such a threshold has to be regarded as a lower cutoff for small stress perturbations in the use of the Coulomb failure model. Indeed, no intrinsic threshold exists for the Coulomb failure model. Considering rate-and-state friction laws, our results show also that no triggering threshold is present (see Figure 5 where the linear behavior extends to very small stress magnitudes).

[57] Before ending this section, we insist on the fact that the parameter $a\sigma_0 \pm = 0.75$ MPa in our model) does not represent the triggering threshold mentioned in the literature [e.g., *King et al.*, 1994] but rather a natural cutoff between small and large amplitudes.

8. Conclusions

[58] Looking at our results, it seems like the Coulomb failure criterion is a good tool for static stress variations. First, the Coulomb failure function $\Delta\text{CFF} = \Delta\tau - \mu_*\Delta\sigma$ is the relevant parameter to account for stress perturbation. All combinations of the normal or shear stress perturbations that correspond to the same ΔCFF lead to the same behavior of the fault. Second, the predictions in terms of clock advance from the Coulomb failure criterion are in agreement to a first order with our results during more than, say, 90% of the earthquake cycle duration (the duration of the locked phase, see Appendix B). We also showed that a triggering threshold for static triggering does not exist in our model as discussed in section 7. The Coulomb failure criterion fails to estimate the clock advance or delay of faults at the end of the seismic cycle (the last 10% of the cycle) when loading (i.e., ΔCFF > 0) or unloading steps (i.e., ΔCFF < 0) are considered, as illustrated by Figure 6. This discrepancy is difficult to test in nature since, on the one hand, negative Coulomb stress changes result in a decrease of the seismicity rate, and are more difficult to observe statistically; indeed, it is easier to detect shocks than "antishocks" [*Harris and Simpson*, 1998]. On the other hand, for clock advance, departure from the Coulomb failure model is hidden by the limit of maximum clock advance $T_{\mathbf{inter}} - t_0$.

[59] Nevertheless, and according to our results, a simple failure criterion such as Coulomb, seems adapted to determine the areas where earthquake triggering is enhanced.

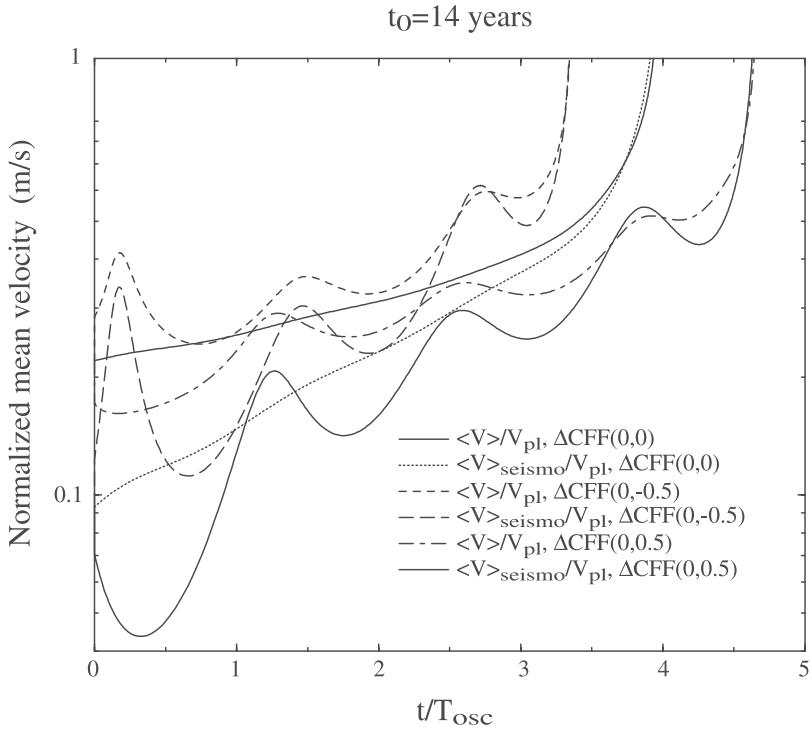

Figure A1. Mean sliding velocity on the fault $\langle V \rangle / V_{pl}$ and in the seismogenic zone $\langle V \rangle_{\text{seismo}} / V_{pl}$ for various change of the Coulomb stress, i.e., ΔCFF(0, 0) = 0 MPa, ΔCFF(0, -0.5) = 0.3 MPa, and ΔCFF(0, 0.5) = -0.3 MPa, applied at time t_0 = 14 years. When the Coulomb stress change are different from zero, the fault response oscillates at a period close to T_{osc} defined in equation (A2).

However, it is unable to give an accurate timing of the occurrence of an earthquakes since no evolution of the slip velocity occurs during the cycle. Such an evolution seems to be responsible for the existence of the Omori law as illustrated by *Dieterich* [1994] or *Ziv and Rubin* [2003]. In particular, the aftershocks duration t_a defined in the model of *Dieterich* [1994] is equal to $t_a = a\sigma_0/\dot{\tau}$ and depends on the frictional parameter a which is equal to zero in a Coulomb failure model, leading to a zero aftershocks duration [*Gomberg et al.*, 2000a]. Therefore we believe that the computation of the Coulomb stress change is useful but has to be coupled to a more realistic fault model such as done by *Toda et al.* [1998] considering rate-and-state friction laws.

Appendix A: Cause of the Oscillations of the Clock Advance During the Earthquake Cycle

[60] We previously noticed looking at Figures 4 and 6 that the clock advance or delay was oscillating throughout the earthquake cycle. Here we analyze the roots of these fluctuations.

[61] Figure A1 presents the mean sliding velocity $\langle V \rangle(t) = 1/(z_2 - z_1)\int_{z_1}^{z_2} V(z, t)\, dz$ along the fault (z_1 = 0 km and z_2 = -20 km) and in the seismogenic zone (that is, for $z_1 = -15$ km and z_2 = -2 km) as a function of time, in response to loading (ΔCFF(0, -0.5) = 0.3 MPa) and unloading steps (ΔCFF(0, 0.5) = -0.3 MPa) applied at time t_0 = 14 years. For the sake of comparison, the unperturbated case ΔCFF(0, 0) = 0 MPa is also shown. Time is normalized by a period T_{osc} which will be defined in equation (A2). We see that in response to loading or unloading steps, the mean velocity oscillates at a period close to T_{osc}. As can be verified looking at Figure A1, these oscillations come mainly from the velocity weakening (or seismogenic) region, although we have also observed some small oscillations at depths greater than 15 km ($z > -15$ km) in the deeper velocity strengthening region.

[62] Considering a spring block model, *Perfettini* [2000] performed a stability analysis around steady state, i.e., when the block slides at the plate velocity V_{pl}. He showed that in response to a small perturbation, the spring slider system presents oscillations when the equivalent stiffness of the fault verifies$k_- < k < k_+$, where k_- and k_+ are given by

$$k_{\pm} = \sigma_0 \left(\sqrt{b} \pm \sqrt{a}\right)^2 / D_c. \tag{A1}$$

The period of the oscillations is given by

$$T_{\text{osc}} = \frac{4\pi a \sigma_0}{V_{pl}\sqrt{(k_+ - k)(k - k_-)}}, \tag{A2}$$

which is used to normalize time in Figure A1. The period T_{osc} represents an intrinsic period of oscillation of the spring-slider system. As may be seen in Figure A1, the amplitude of these oscillations is decreasing with the time elapsed since the stress step. We believe that the oscillations observed in Figures 4 and 6 are due to the oscillatory response of the fault to stress perturbations displayed in Figure A1. When a stress step is applied early in the cycle, time to instability is long (i.e., long t_p) and perturbations have vanished at the onset of instability. Therefore no oscillation are visible for early triggering (i.e., small t_0). On the contrary, for late triggering (i.e., $t_0 \simeq T_{\text{inter}}$), oscillations

in sliding velocity (with time) are still significant at the instability onset. Accordingly, fluctuations of the clock change with t_0 are important for late triggering.

[63] Choosing $a = 0.015$ and $b = 0.019$ as representative values in the seismogenic zone, taking $L = 10$ km as being the width of this area, one finds $T_{osc} \simeq 18.1$ years using the expression of the stiffness of a fault given in equation (16). This value is in agreement with the period of the oscillations observed in Figure A1.

Appendix B: Effect of a Sudden Stress Change

B1. Velocity Change Due to a Sudden Stress Change

[64] We estimate the velocity change due to a step in shear and normal stress. For the sake of simplicity, the spring slider model will be used in the quasi-static limit:

$$\tau = \tau_0 + \dot{\tau} t - k\delta, \tag{B1}$$

where τ_0 is the initial shear stress, $\dot{\tau} = kV_{pl}$ is the stressing rate, V_{pl} is the plate velocity, and δ is the accumulated slip.

[65] Suppose that at time t_0, the shear and normal stress jump instantaneously from τ_0 and σ_0 to $\tau_1 = \tau_0 + \Delta\tau$ and $\sigma_1 = \sigma_0 + \Delta\sigma$. As previously noted by *Dieterich* [1994], a change in normal stress from σ_0 to σ_1 results in an immediate change of the state variable from θ_0 to θ_1 with

$$\theta_1 = \theta_0 \left(\frac{\sigma_1}{\sigma_0}\right)^{-\alpha/b}, \tag{B2}$$

which directly arises from equation (5). The initial shear stress τ_0, for a fault sliding at any velocity V_0 is

$$\tau_0 = \sigma_0\left[\mu_* + a\log\left(V_0/V_*\right) + b\log\left(\theta_0/\theta_*\right)\right] \tag{B3}$$

and becomes τ_1 after the shear and normal stress steps:

$$\tau_1 = \sigma_1\left[\mu_* + a\log\left(V_1/V_*\right) + b\log\left(\theta_1/\theta_*\right)\right] \tag{B4}$$

where V_1 is the velocity right after the application of the steps. Subtracting equation (B3) from equation (B4) and introducing equation (B2) leads to

$$\begin{aligned}\Delta\tau &= \tau_1 - \tau_0 \\ &= \sigma_1 a\log(V_1/V_0) + \left(\mu_* + a\log\left(V_0/V_*\right)\right. \\ &\quad \left. + b\log\left(\theta_0/\theta_*\right)\right)\Delta\sigma - \alpha\sigma_1\log(\sigma_1/\sigma_0).\end{aligned} \tag{B5}$$

Introducing the Coulomb stress $\Delta\mathrm{CFF}^0 = \Delta\tau - \mu_0\Delta\sigma$ at the onset of the steps, where $\mu_0 = \tau_0/\sigma_0$ is the initial coefficient of friction, we obtain the sliding velocity immediately after the steps:

$$V_1 = V_0\left(\frac{\sigma_1}{\sigma_0}\right)^{\alpha/a} \exp\left[\Delta\mathrm{CFF}^0/(a\sigma_1)\right], \tag{B6}$$

which leads to a relative velocity change $\Delta V/V_0 = (V_1 - V_0)/V_0$:

$$\frac{\Delta V}{V_0} = \left(\frac{\sigma_1}{\sigma_0}\right)^{\alpha/a} \exp\left[\Delta\mathrm{CFF}^0/(a\sigma_1)\right] - 1. \tag{B7}$$

For small stress perturbations, namely, $\Delta\mathrm{CFF}^0 \ll a\sigma_0$ and $\Delta\sigma \ll \sigma_0$, equation (B7) becomes

$$\frac{\Delta V}{V_0} \simeq \frac{\Delta\tau - (\mu_0 - \alpha)\Delta\sigma}{a\sigma_0}. \tag{B8}$$

B2. Rate and State Versus Coulomb

[66] We show here that the rate and state formalism reduces to a Coulomb failure model during the phase where the fault is at rest ($\dot{\delta} \to 0$). This phase is referred to as the locked phase.

[67] Mathematically, the fault is defined as being locked when $V\theta/D_c \ll 1$ so that prior to the stress steps, equation (5) reduces to $\dot{\theta} \simeq 1$. This leads to $\theta \simeq \theta_0 + t$, where θ_0 is the value of the state variable at the origin of time for which there is no initial displacement ($\delta(0) = 0$). The accumulated displacement during the locked phase is negligible since the sliding velocities involved are extremely low compared to the plate velocities. In this case, equation (B1) becomes

$$\sigma\left[\mu'_* + a\log(V) + b\log(\theta)\right] = \tau_0 + \dot{\tau} t, \tag{B9}$$

with $\mu'_* = \mu_* - a\log(V_*) - b\log(\theta_*)$. Introducing the initial velocity $V(0) = V_0$, equation (B9) reads, using $\theta \simeq \theta_0 + t$,

$$\sigma[a\log(V/V_0) + b\log(1 + t/\theta_0)] = \dot{\tau} t, \tag{B10}$$

leading to

$$\log(V/V_0) = \dot{\tau} t/(a\sigma) - b/a\log(1 + t/\theta_0). \tag{B11}$$

The second term on the right-hand side has a logarithmic dependence with time and therefore is negligible compared to the linear term $\dot{\tau} t/(a\sigma)$. Therefore a relative change of velocity from $\Delta V/V$ is approximately equal to

$$\Delta V/V = \dot{\tau}\Delta t/(a\sigma). \tag{B12}$$

Using equation (B8), we find that for Coulomb stress changes of small amplitudes ($\Delta\mathrm{CFF} \ll a\sigma_0$ and $\Delta\sigma \ll \sigma_0$):

$$\dot{\tau}\Delta t/(a\sigma) = \frac{\Delta\tau - (\mu_0 - \alpha)\Delta\sigma}{a\sigma_0}, \tag{B13}$$

leading to

$$\Delta t = \frac{\Delta\tau - (\mu_0 - \alpha)\Delta\sigma}{\dot{\tau}}. \tag{B14}$$

This prediction is in agreement with the prediction of a Coulomb failure model considering a static coefficient of friction $\mu_s = \mu_0 - \alpha$. In our model where the steps are not applied abruptly but over a time interval of order 10 s, the influence of the α term is negligible (see *Perfettini et al.* [2003] for a discussion of the influence of α). Therefore we expect equation (B14) to transform in our study in

$$\Delta t = \frac{\Delta\tau - \mu_0\Delta\sigma}{\dot{\tau}}. \tag{B15}$$

[68] As previously demonstrated by *Gomberg et al.* [2000a] but considering only shear stress variations, a fault governed by rate and state friction laws is Coulomb-like

during the locked phase. Since the fault is only accelerating at the very end of the earthquake cycle, we can consider that during most of its life the fault is essentially locked, behaving like in a Coulomb failure model. This explains why during more than 90% of the earthquake cycle, the predictions of the Coulomb failure model are fairly close to the results of our model.

Appendix C: Analytical Derivation of the Time to Instability for Shear Stress Perturbations

C1. General Derivation

[69] The derivation of the time to instability we present here extend the one presented originally by *Dieterich* [1992]. We consider a fault of stiffness k loaded at a constant rate $\dot{\tau} = kV_{pl}$ where V_{pl} is the plate velocity. In addition to this constant loading rate, we add an arbitrary change in shear stress $\Delta\tau(t)$. To estimate analytically the time to instability, it is reasonable to neglect the effect of the radiation damping term which becomes only active at high velocities (inertial effects become significant only at velocities of the order or higher than 10^{-3} m/s as discussed by *Roy and Marone* [1996]). The error done neglecting this term is negligible compared to the time to instability t. In that case, the quasi-static equation governing the evolution of the fault is

$$\tau_f = \tau_0 + \dot{\tau}t - k\delta + \Delta\tau(t), \tag{C1}$$

where τ_0 is the preexisting shear stress on the fault and τ_f is the frictional stress τ_f which obeys

$$\tau_f = \sigma_0\left[\mu_* + a\ln\left(V/V_*\right) + b\ln\left(\theta/\theta_*\right)\right]. \tag{C2}$$

The evolution of the state variable θ is governed by the Dieterich evolution law:

$$\frac{d\theta}{dt} = 1 - \frac{V\theta}{D_c}. \tag{C3}$$

Equation (C3) can be integrated, giving

$$\theta(t) = \theta_0[1 + C(t)]\exp\left(-\delta(t)/D_c\right) \tag{C4}$$

with $C(t)$ being given by

$$C(t) = \frac{1}{\theta_0}\int_0^t \exp\left(\delta(u)/D_c\right)du, \tag{C5}$$

and θ_0 is the value of the state variable at time $t = 0$.

[70] For $V \to 0$, the state variable can be identified as the time of contact between the two sides of the faults, i.e., the elapsed time since the last earthquake on this fault. Therefore, for a fault late in the earthquake cycle, we can identify θ as the interseismic time. In this case, the ratio $V\theta/D_c$ is much greater than one when the sliding velocity verifies $V \gg D_c/\theta$. Taking θ 100 years and $D_c = 10^{-2}$ cm, the last inequality leads to $V \gg 3\ 10^{-10}$ m/s, and is verified at the end of the earthquake cycle where the sliding velocity becomes significant. If $V\theta/D_c \gg 1$, equation (C3) becomes

$$\frac{d\theta}{dt} \simeq -\frac{V\theta}{D_c}, \tag{C6}$$

which can easily be integrated, giving

$$\theta(\delta) = \theta_0\exp\left(-\delta/D_c\right). \tag{C7}$$

This form was originally proposed by *Dieterich* [1992] and is identical to the one given in equation (C4) providing $C(t) \ll 1$. As discussed earlier, such an approximation is valid for faults late in the earthquake cycle (large θ_0). It is to be noted that the expression of the state variable given in equation (C4) is the exact solution of equation (C3) and remains valid throughout the whole earthquake cycle. Equation (C4) can be combined with equations (C1) and (C2) yielding

$$\sigma_0\left[\mu_* + a\ln\left(V/V_*\right) + b\ln\left(\theta_0/\theta_*\right) - \frac{b\delta}{D_c} + b\ln\left[1 + C(t)\right]\right] = \tau_0 + \dot{\tau}t - k\delta + \Delta\tau(t). \tag{C8}$$

In order to write equation (C8) in a more condensed way, we introduce the H parameter of *Dieterich* [1992]:

$$H = \frac{b}{D_c} - \frac{k}{\sigma_0}. \tag{C9}$$

Equation (C8) can now be written as

$$\ln V = \frac{\tau_0/\sigma_0 - \mu'_* - b\ln\left[\theta_0(1 + C(t))\right]}{a} + \frac{H\delta}{a} + \frac{\dot{\tau}t + \Delta\tau(t)}{a\sigma_0}, \tag{C10}$$

where the parameter $\mu'_* = \mu_* - a\ln V_* - b\ln\theta_*$ has been introduced. Noting that, assuming $\delta(0) = 0$,

$$\ln\dot{\delta}_0 = \frac{\tau_0/\sigma_0 - \mu'_* - b\ln\theta_0}{a}, \tag{C11}$$

where $\dot{\delta}_0$ is the initial slip velocity, equation (C10) yields

$$\dot{\delta} = \dot{\delta}_0\exp\left[H\delta/a\right]\exp\left[\left(\dot{\tau}t + \Delta\tau(t)\right)/(a\sigma_0)\right]\cdot\left[1 + C(t)\right]^{-b/a}. \tag{C12}$$

The integration can be then be carried on:

$$\dot{\delta}_0\int_0^t \left[1 + C(y)\right]^{-b/a}\exp\left[\left(\dot{\tau}y + \Delta\tau(y)\right)/(a\sigma_0)\right]dy = \int_0^\delta \exp\left[-Hu/a\right]du. \tag{C13}$$

Let us introduce the function $F(t)$ as

$$F(t) = \dot{\delta}_0\int_0^t \left[1 + C(y)\right]^{-b/a}\exp\left[\left(\dot{\tau}y + \Delta\tau(y)\right)/(a\sigma_0)\right]dy. \tag{C14}$$

The right-hand side of equation (C13) can be easily integrated giving

$$\delta = -\frac{a}{H}\ln\left[1 - \frac{HF(t)}{a}\right]. \tag{C15}$$

We can now easily determine the slip velocity $\dot{\delta}$:

$$\dot{\delta} = \frac{dF/dt}{1 - \frac{HF(t)}{a}}. \tag{C16}$$

The time to instability t_p can be estimated as the time for which the slip velocity becomes infinite or equivalently $\dot{\delta}^{-1} \rightarrow 0$. Using equation (C16), this can be formulated as

$$F(t_p) = \frac{a}{H}. \tag{C17}$$

C2. General Comments on the Time to Instability t_p

[71] Even though equation (C17) cannot be usually solved analytically because $F(t)$ does not have, in most cases, an analytical expression, some general statements can be expressed. First of all, the integrand in the expression of $F(t)$ given in equation (C14) is always positive. This states that $F(t) > 0$ for $t > 0$ while it is trivial to see that $F(0) = 0$. Therefore equation (C17) has a meaning (and an infinite velocity is reached, hence an instability occurs) only for $H > 0$. This condition is met when $k < b\sigma_0/D_c$ as already noted by *Dieterich* [1992]. For a sufficiently large fault ($h \gg h_c$ or equivalently $k \ll k_c$), the last condition is fulfilled.

[72] Furthermore, the function F is growing with time. This can easily be checked by derivation of equation (C14) with respect to time:

$$\frac{dF}{dt}(t) = \dot{\delta}_0[1 + C(t)]^{-b/a} \exp\left[(\dot{\tau}t + \Delta\tau(t))/(a\sigma_0)\right] > 0. \tag{C18}$$

These last two remarks are useful to derive an important property of the time to instability, as illustrated schematically in Figure C1. Let β be a parameter of the function F such as a, σ_0, $\dot{\tau}$, etc. The fact that $F(t)$ is a growing function of time implies that $t_p(\beta_1) > t_p(\beta_2)$ for $F(\beta_2) > F(\beta_1)$. Therefore, if F is an increasing (resp. decreasing) function of β, the time to instability is a decreasing (respectively increasing) function of β.

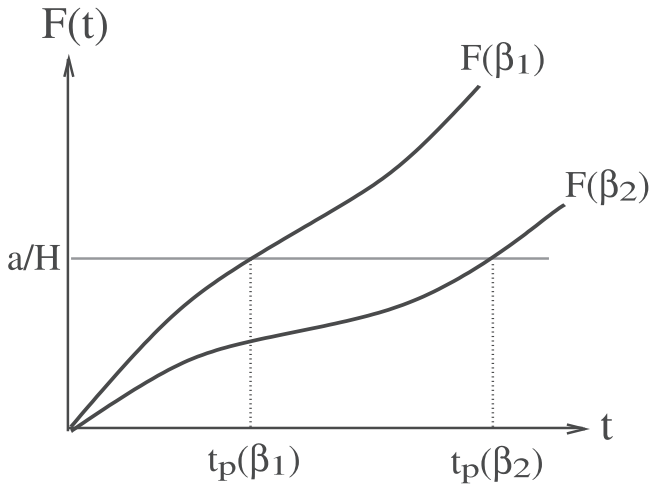

Figure C1. Graphic method to solve equation (C17). For a given value of the parameter α_i, $i = 1, 2$, the intersection of the growing function with time $F(\alpha_i)(t)$ with the line a/H gives the time to instability $t_p(\alpha_i)$. The inequality $F(\alpha_2) > F(\alpha_1)$ is equivalent to $t_p(\alpha_1) > t_p(\alpha_2)$.

Appendix D: Applications

[73] In this appendix, we assume $V\theta/D_c \gg 1$, i.e., $C(y)$ can be neglected in (C14), an assumption that is valid for a fault late in the earthquake cycle (see Appendix C). We also use the notation $\gamma = \dot{\tau}/(a\sigma_0)$, which the inverse of the aftershock duration $t_a = a\sigma_0/\dot{\tau}$ defined by *Dieterich* [1994].

D1. Case of No Stress Perturbations

[74] When there are no perturbations of the shear stress ($\Delta\tau(t) = 0$), equation (C14) gives

$$F(t) = \frac{\dot{\delta}_0}{\gamma}\left[\exp\left(\dot{\tau}t/(a\sigma_0)\right) - 1\right], \tag{D1}$$

and the time to instability t_f can be obtained combining equation (D1) together with equation (C17):

$$t_f = \frac{1}{\gamma}\ln\left[1 + \dot{\tau}/\left(\sigma_0 H\dot{\delta}_0\right)\right], \tag{D2}$$

which is equivalent to the previous estimate of *Dieterich* [1992].

D2. Case of a Shear Stress Step

[75] We now consider a shear stress step of constant amplitude $\Delta\tau$ applied at time t_0 (i.e., $\Delta\tau(t) = \Delta\tau\, H(t - t_0)$, where $H(t)$ is the Heaviside function). In this case we have

$$F(t) = \frac{\dot{\delta}_0}{\gamma}\left[\exp\left(\gamma t_0\right) - 1 + \exp[\Delta\tau/(a\sigma_0)]\left(\exp\left(\gamma t\right) - \exp\left(\gamma t_0\right)\right)\right], \tag{D3}$$

so that the time to instability, t_p, which satisfies $F(t_p) = a/H$, is given by

$$t_p = -\frac{\Delta\tau}{\dot{\tau}} + \frac{1}{\gamma}\log\left[1 + \frac{\gamma a}{\dot{\delta}_0 H} - \exp(\gamma t_0)\left(1 - \exp[\Delta\tau/(a\sigma_0)]\right)\right], \tag{D4}$$

which leads, using equation (D2), to the clock advance:

$$\Delta t = t_f - t_p = \frac{\Delta\tau}{\dot{\tau}} - \frac{1}{\gamma}\quad \log\left[1 - \exp\left(\gamma t_0\right)\frac{1 - \exp[\Delta\tau/(a\sigma_0)]}{1 + \frac{\gamma a}{\dot{\delta}_0 H}}\right]. \tag{D5}$$

This formula was previously obtained by *Gomberg et al.* [1998].

D2.1. Limit of Small Amplitudes

[76] For steps of small amplitude, i.e., $\Delta\tau \ll a\sigma_0$, equation (D5) becomes

$$\Delta t = \frac{\Delta\tau}{\dot{\tau}}\left[1 - \frac{\exp(\gamma t_0)}{1 + \frac{\gamma a}{\dot{\delta}_0 H}}\right]. \tag{D6}$$

D2.2. Limit of Large Amplitudes

[77] In the case where $\Delta\tau \gg a\sigma_0$, equation (D5) becomes

$$\Delta t = t_f - t_0 \tag{D7}$$

meaning that triggering is instantaneous.

[78] Using equation (D5), the case $-\Delta\tau \gg a\sigma_0$ leads to

$$\Delta t = \frac{\Delta\tau}{\dot{\tau}} - \frac{1}{\gamma}\log\left[1 - \frac{\exp(\gamma t_0)}{1 + \frac{\gamma a}{\dot{\delta}_0 H}}\right]. \tag{D8}$$

[79] **Acknowledgments.** A special thank to J. R. Rice, who originally motivated this work. We are grateful to C. Marone and S. Nielsen for their thoughtful review and suggestions. We are very grateful to M. Bouchon, R. Archuleta, N. Lapusta, and J.-P. Ampuero for numerous discussions. A part of this study was funded by the ACI "Risques Naturels" and ACI

"Jeunes Chercheurs" and the computations presented in this paper were performed at the Service Commun de Calcul Intensif de l'Observatoire de Grenoble (SCCI). A.C. thanks ASSEDIC for its support.

References

Baumberger, T., P. Berthoud, and C. Caroli, Physical analysis of the state- and rate-dependent friction law, II. Dynamic friction, *Phys. Rev. B*, *60*, 3928–3939, 1999.

Bilby, B. A., and J. D. Eshelby, Dislocations and theory of fracture, in *Fracture, an Advanced Treatise*, vol. I, edited by H. Liebowitz, pp. 99–182, Academic, San Diego, Calif., 1968.

Blanpied, M. L., D. A. Lockner, and J. D. Byerlee, Fault stability inferred from granite sliding experiments at hydrothermal conditions, *Geophys. Res. Lett.*, *18*(4), 609–612, 1991.

Bouchon, M., H. Sekiguchi, K. Irikura, and T. Iwata, Some characteristics of the stress field of the 1995 Hyogo-ken Nambu (Kobe) earthquake, *J. Geophys. Res.*, *103*, 24,271–24,282, 1998.

Bowden, F. P., and D. Tabor, *The Friction and Lubrification of Solids, Part I*, Clarenden Press, Oxford, U.K., 1950.

Bowden, F. P., and D. Tabor, *The Friction and Lubrification of Solids, Part II*, Clarenden Press, Oxford, U.K., 1964.

Brudy, M., M. D. Zoback, K. Fuchs, F. Rummel, and J. Baumgaertner, Estimation of the complete stress tensor to 8 km depth in the KTB scientific drill holes: Implications for crustal strength, *J. Geophys. Res.*, *102*, 18,453–18,475, 1997.

Chambon, G., J. Schmittbuhl, and A. Corfdir, Laboratory gouge friction: Seismic-like slip weakening and secondary rate-and state-effects, *Geophys. Res. Lett.*, *29*(10), 1366, doi:10.1029/2001GL014467, 2002.

Dieterich, J. H., Modeling of rock friction: 1. Experimental results and constitutive equations, *J. Geophys. Res.*, *84*, 2161–2168, 1979.

Dieterich, J. H., Constitutive properties of faults with simulated gouge, in *Mechanical Behavior of Crustal Rocks*, *Geophys. Monogr. Ser.*, vol. 24, edited by N. L. Carter et al., pp. 103–120, AGU, Washington, D. C., 1981.

Dieterich, J. H., Earthquake nucleation on faults with rate- and state-dependent strength, *Tectonophysics*, *211*, 115–134, 1992.

Dieterich, J. H., A constitutive law for rate of earthquake production and its application to earthquake clustering, *J. Geophys. Res.*, *99*, 2601–2618, 1994.

Dieterich, J. H., and B. D. Kilgore, Imaging surface contacts: power law contact distribution and contact stresses in quartz, calcite, glass and acrylic plastic, *Tectonophysics*, *256*, 219–239, 1994.

Gomberg, J., and P. Bodin, Triggering of the Little Skull Mountain Nevada earthquake with dynamic strains, *Bull. Seismol. Soc. Am.*, *84*, 844–853, 1994.

Gomberg, J., and S. Davis, Stress/strain changes and triggered seismicity at The Geysers, California, *J. Geophys. Res.*, *101*, 733–750, 1996.

Gomberg, J., N. M. Beeler, M. L. Blanpied, and P. Bodin, Earthquake triggering by transient and static deformations, *J. Geophys. Res.*, *103*, 24,411–24,426, 1998.

Gomberg, J., N. M. Beeler, and M. L. Blanpied, On rate-state and Coulomb failure models, *J. Geophys. Res.*, *105*, 7857–7871, 2000a.

Gomberg, J., P. A. Reasenberg, P. Bodin, and R. H. Harris, Triggering of eartquake aftershocks by dynamic stresses, *Nature*, *408*, 570–573, 2000b.

Gomberg, J., P. A. Reasenberg, P. Bodin, and R. H. Harris, Earthquake triggering by seismic waves following the Landers and Hector Mine earthquake, *Nature*, *411*, 462–466, 2001.

Harris, R. A., Introduction to special section: Stress triggers, stress shadows, and implications for seismic hazard, *J. Geophys. Res.*, *103*, 24,347–24,358, 1998.

Harris, R. A., and R. W. Simpson, Suppression of large earthquakes by stress shadows: A comparison of Coulomb and rate-and-state failure, *J. Geophys. Res.*, *103*, 24,439–24,451, 1998.

Ide, S., and M. Takeo, Determination of constitutive relations of fault slip based on seismic wave analysis, *J. Geophys. Res.*, *102*, 27,379–27,391, 1997.

King, G. C. P., R. S. Stein, and J. Lin, Static stress changes and the triggering of earthquakes, *Bull. Seismol. Soc. Am.*, *84*, 935–953, 1994.

Lapusta, N., and J. R. Rice, Nucleation and early seismic propagation of small and large events in a crustal earthquake model, *J. Geophys. Res.*, *108*(B4), 2205, doi:10.1029/2001JB000793, 2003.

Lapusta, N., J. R. Rice, Y. Ben-Zion, and G. Zheng, Elastodynamic analysis for slow tectonic loading with spontaneous rupture episodes on faults with rate-and state-dependent friction, *J. Geophys. Res.*, *105*, 23,765–23,789, 2000.

Linker, M. F., and J. H. Dieterich, Effects of variable normal stress on rock friction: Observations and constitutive equations, *J. Geophys. Res.*, *97*, 4923–4940, 1992.

Marone, C., Laboratory-derived friction laws and their application to seismic faulting, *Annu. Rev. Eath Planet. Sci.*, *26*, 643–696, 1998.

Marone, C., and B. Kilgore, Scaling of the critical slip distance for seismic faulting with shear strain in fault zones, *Nature*, *362*, 618–621, 1993.

Marone, C. J., C. H. Scholz, and R. Bilham, On the mechanics of earthquake afterslip, *J. Geophys. Res.*, *96*, 8441–8452, 1991.

Perfettini, H., Frottement sur une faille: influence des fluctuations de la contrainte normale, Ph.D. thesis, Univ. Pierre et Marie Curie, Paris, 2000.

Perfettini, H., J. Schmittbuhl, J. R. Rice, and M. Cocco, Frictional response induced by time-dependent fluctuations of the normal loading, *J. Geophys. Res.*, *106*, 13,455–13,472, 2001.

Perfettini, H., J. Schmittbuhl, and A. Cochard, Shear and normal load perturbations on a two-dimensional continuous fault: 2. Dynamic triggering, *J. Geophys.*, 108, doi:10.1029/2002JB001805, in press, 2003.

Persson, B. N. J., *Sliding Friction: Physical Principles and Applications*, Springer-Verlag, New York, 1998.

Press, W. H., B. P. Flannery, S. A. Teukolsky, and W. T. Vetterling, Integration of ordinary differential equations, in *Numerical Recipes in C, The Art of Scientific Computing*, 2nd ed., pp. 707–752, Cambridge Univ. Press, New York, 1992.

Rice, J. R., Fault stress states, pore pressure distributions, and the weakness of the San Andreas fault, in *Fault Mechanics and Transport Properties of Rocks*, edited by B. Evans and T.-F. Wong, pp. 475–503, Academic, San Diego, Calif., 1992.

Rice, J. R., Spatio-temporal complexity of slip on a fault, *J. Geophys. Res.*, *98*, 9885–9907, 1993.

Rice, J. R., and A. L. Ruina, Stability of steady frictional slipping, *J. Appl. Mech.*, *50*, 343–349, 1983.

Richardson, E., and C. J. Marone, Effects of normal stress vibrations on frictional healing, *J. Geophys. Res.*, *104*, 28,859–28,878, 1999.

Roy, M., and C. Marone, Earthquake nucleation on model faults with rate - and state-dependent friction: Effects of inertia, *J. Geophys. Res.*, *101*, 13,919–13,932, 1996.

Ruina, A. L., Slip instability and state variable fricton laws, *J. Geophys. Res.*, *88*, 10,359–10,370, 1983.

Stein, R., A. Barka, and J. Dieterich, Progressive failure on the North Anatolian fault since 1939 by earthquake stress triggering, *Geophys. J. Int.*, *128*, 594–604, 1997.

Stuart, W. D., and T. E. Tullis, Fault model for preseismic deformation at Parkfield, California, *J. Geophys. Res.*, *100*, 24,079–24,099, 1995.

Toda, S., S. R. Stein, P. A. Reasenberg, and J. H. Dieterich, Stress transferred by the M_w = 6.9 Kobe, Japan, shock: Effect on aftershocks and future earthquake probabilities, *J. Geophys. Res.*, *103*, 24,543–24,565, 1998.

Tse, S. T., and J. R. Rice, Crustal earthquake instability in relation to the depth variation of frictional slip properties, *J. Geophys. Res.*, *91*, 9452–9472, 1986.

Uenishi, K., and J. R. Rice, Universal nucleation length for slip-weakening rupture instability under nonuniform fault loading, *J. Geophys. Res.*, *108*(B1), 2042, doi:10.1029/2001JB001681, 2003.

Ziv, A., and A. Rubin, Static stress transfer and earthquake triggering: No lower threshold in sight?, *J. Geophys. Res.*, *105*, 13,361–13,642, 2000.

Ziv, A., and A. M. Rubin, Implications of rate-and-state friction for properties of aftershock sequence: Quasi-static inherently discrete simulations, *J. Geophys. Res.*, *108*(B1), 2051, doi:10.1029/2001JB001219, 2003.

A. Cochard, 14, rue Fagon, F-75013 Paris, France. (cochard@esag.harvard.edu)

H. Perfettini, Laboratoire de Géophysique Interne et Tectonophysique, BP 53X, F-38041 Grenoble Cedex, France. (Hugo.Perfettini@obs.ujf-grenoble.fr)

J. Schmittbuhl, Laboratoire de Géologie UMR 8538, Ecole Normale Supérieure, 24, rue Lhomond, F-75231 Paris cedex 05, France. (Jean.Schmittbuhl@ens.fr)